# HEAT AND REACTION CHARACTERISTICS OF MULTI-STAGE ALCOHOLIC-FUEL REFORMER

*K. Tatsumi[1], K. Kuwabara[1], Y. Rai[1] and K. Nakabe[1]*

[1] Department of Mechanical Engineering and Science,
Kyoto University, Kyoto, 606-8501 JAPAN

## ABSTRACT

A compact multi-stage alcoholic fuel reformer, which is composed of multiple ports of reactant supply, is proposed and examined. The temperature, flow velocity and exhaust gas components of the multi-stage reformer were measured, and the effects of stage number, equivalence ratios, fuel flow rate and load change on the reforming characteristics were discussed. Particularly, by increasing the stage number, $H_2$ concentration increased by 10%, and a significant increase of the local temperature in the reformer was also avoided.

## INTRODUCTION

Hydrogen is considered to be one of the essential fuels to be used in the next-generation power supplies; such as fuel cells, micro gas turbines and internal combustion engines. However, during the transition period until the infrastructure of hydrogen supply is developed, an on-site hydrogen fuel production system should be provided as the alternative. This requires the development of a high-efficiency and compact fuel reforming system, by which hydrocarbon fuels are converted to hydrogen rich synthesis gas. To put this system into practical use, however, we must tackle the problems such as load fluctuation, variation of fuel aspect and low conversion efficiency [1, 2].

From these motivations, a multi-stage fuel reformer, which is composed of multiple ports of reactant supply, is proposed and examined in the present study. By multiplying the reaction stages, the local heat balance and temperature inside this reformer can effectively and quickly be controlled, resulting in quick response to load change, enhancement of the reforming effectiveness and reduction of the undesired exhausts such as soot or CO [1, 3-5]. The multi-stage fuel and air supply also enables the temperature control of the reformer, which is important in the meanings of the thermal durability of the device itself.

In this paper, results of a prototype multi-stage tube type reformer are reported. Methanol was used as fuel in the present experiment. Alcohol is relatively easy to transport and storage since it is chemically stable and is in liquid phase under atmospheric temperature and pressure. It is, therefore, considered to be suitable to compact energy supply systems with an output of several kilo watts [6]. No catalyst was mounted on the reformer in this study. It is reported that the thermal condition of the reformer largely affects the reforming performance in either case: with and without the catalyst [7, 8]. As the initial step of evaluating the multi-stage reformer, therefore, the experiment was conducted without inserting the catalyst to separate the effects of the catalyst characteristics from those of multiplying the reaction stages.

The reformer temperature and exhaust gas components were measured, and the effects of stage number, equivalence ratios, fuel flow rate, load change, on the reforming characteristics are discussed, mainly focusing on the partial oxidation reaction (POR).

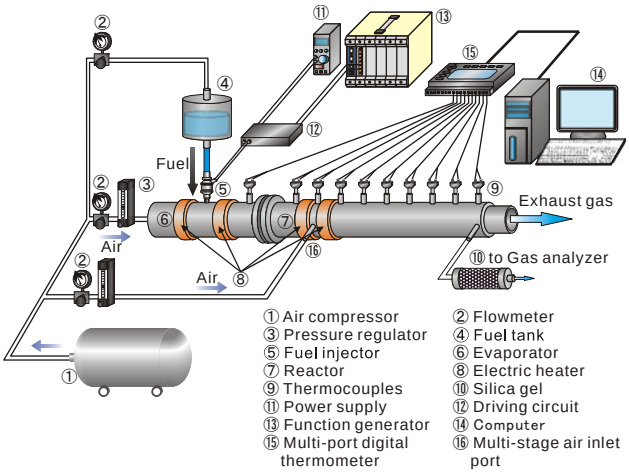


Fig. 1. Schematic view of the experimental setup.

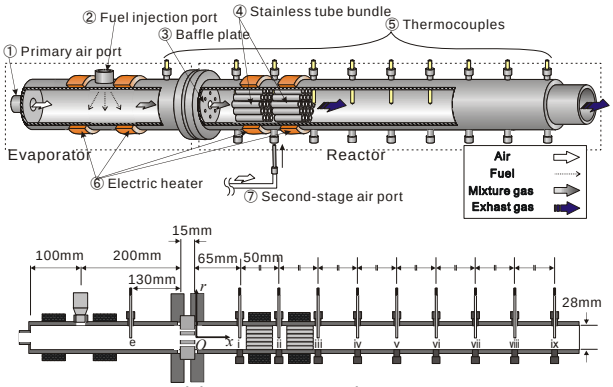


(a) Evaporator and reactor

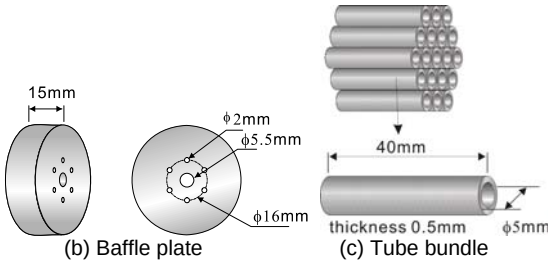


(b) Baffle plate (c) Tube bundle

Fig. 2. Schematic view of reformer.

## EXPERIMENTAL PROCEDURE

Figure 1 shows the present experimental apparatus to evaluate the multi-stage methanol fuel reformer. Figure 2(a) illustrates the schematic and cross-sectional views of the reformer. As shown in the figure, the reformer was composed of two parts, i.e., the evaporator and reactor.

The evaporator was made of a galvanized steel pipe with the inner diameter and length of 28mm and 200mm, respectively. A fuel supply port was located at the side surface, into which an injector with electric valve was mounted. An electric signal was sent from a function generator (Yokogawa; WE500, WE7281) to this injector to control the valve opening. The flow rate of the fuel jet was, therefore, controlled by adjusting the frequency and duty ratio of the signal to a certain value. An air supply port was set at the upstream end of the evaporator. Air supplied to this port was provided from a compressor, and the flow rate was controlled by flow meter and valve (Kofloc; RK1250). At the upstream and downstream areas in adjacent to the fuel supply port, electric band heaters (Sakaguchi E.H. Voc.; BH3430) were wrapped around the pipe. This heater was powered by a voltage slider (Yamabishi; V-130-3) and heated the evaporator wall up to a specified temperature. Thus, the fuel injected from the fuel supply port impinged the pipe inner wall, and was vaporized. The vaporized fuel joining the air flowing from the upstream of the pipe, was then supplied to the reactor through a baffle plate.

As shown in Fig. 2(a), this baffle plate was located between the evaporator and reactor, and multiple holes were drilled in the plate. The configuration of the holes is shown in Fig. 2(b), i.e., a 5.5mm hole was located at the center and 6 holes with 2mm diameter surrounded the center one. This multi-hole baffle plate was expected to enhance the mixing between the vaporized fuel and air, and to prevent backfire from the reactor to the evaporator.

The reactor was made of a stainless steel pipe 28mm in diameter and 500mm in length. In the areas of $70 \le x \le 110$mm and $120 \le x \le 160$mm, bundles of stainless tubes (tube diameter=4mm, length=40mm; see Fig.2(c)) were inserted. These tubes were expected to enhance the reaction efficiency and also produce a stable reaction under high equivalent ratio by enhancing the heat transfer at the tube walls. Band heaters (Watlow; MB01E1AB3005) were attached to the pipe sidewall at each location identical to that where the tube bundles were inserted. These heaters were powered by a voltage slider in the same way as those in the evaporator, and the pipe wall was preheated before the experiment started.

Several loading ports were applied to the sidewalls of the evaporator and reactor at the locations shown in Fig. 2(a). Probes for temperature measurement made of K type thermocouples were inserted into the pipe through these ports. This probe was a two-hole ceramic tube (tube diameter=3mm) having the weld spot of the thermocouples exposed at the tip. To protect the exposed parts of the thermocouples from the flame and reactive gas, and also to prevent any catalysis effects, the thermocouples were coated by silica-particles by burning them with town gas into which Hexamethyldisiloxane was mixed. The signals from the thermocouples were recorded by a personal computer through a digital multi-thermometer (Keyence; NR-1000). The sampling rate and accuracy of the temperature measurement was 1s and ±1°C, respectively.

Gas sampling for gas analysis was conducted by inserting a sampling probe into one of the loading ports. The probe was made of stainless tube 2mm in diameter,

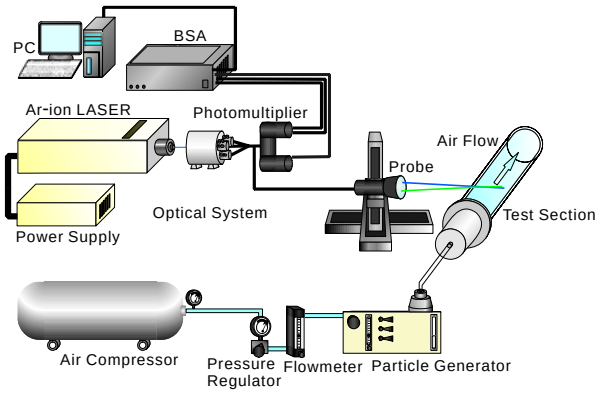


Fig. 3. Schematic view of LDV measurement.

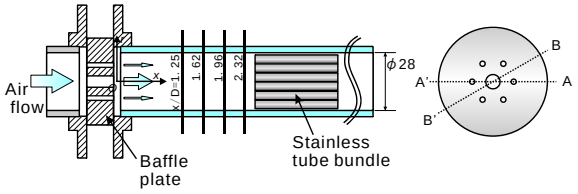


Fig. 4. Cross-sectional view of the measuring region.

to which a 0.3mm hole was applied at the end. The position of the tip end was set at the reactor centerline, and the gas was collected by connecting the tube to a vacuum-collecting chamber. The collected gas was then supplied to a gas chromatograph (Shimadzu; GC-8A) through a filtering chamber packed with silica gel, by which water and unburned methanol were collected. A component detector on the basis of TCD (Thermal Conductivity Detector) method was applied to the gas chromatography. The column (Shinwa chem.; Shincarbon ST) mounted in the chromatograph was calibrated for $H_2$, $N_2$, $O_2$, CO, $CO_2$ gases. Ar gas was used as the carrier gas.

Additional air was also supplied through these ports to the reactor operated in the way of multi-stage reforming. The end of the air-feed tube was located at the central axis of the reactor, and two holes were made at the sidewall of the tube tip, from which air was injected to the reactor in the radial direction.

Measurements using LDV (Laser Doppler Velocimetry) were also conducted to evaluate the velocity field in the reactor. The experimental apparatus is shown in Fig. 3. In this case, a test section different from that used in the aforementioned experiment accompanying reactions and temperature measurements was applied. An acrylic pipe of the same size with the reactor shown in Fig. 2 was made where an optical measurement from the sidewall was available. This pipe was attached to the same evaporator and baffle plate shown in Fig. 2. Air with the flow rate equal to the total value of the air and fuel supplied to the evaporator in the reaction experiment was provided to the upstream end of the evaporator. In the upstream of the evaporator, a particle generator (TSI; six-jet atomizer 9306) was attached and tracing particles of oil mist (DEHS: Di-Ethyl-Hexyl-Sebacate $C_{26}H_{50}O_4$, nominal diameter 1μm) was mixed in the air. In the optical system of the LDV, the laser produced by an argon-ion laser system (Spectra

Physics; model 2017L-AR) having a wavelength of 514.5nm was used together with a beam splitter coupled with a Bragg cell to detect backward flows. The Doppler burst signals from the back-scattering light of the particles were recorded and analyzed by a signal processor (DANTEC; BSA F50), which was linked to and controlled by a personal computer.

The procedure applied in the reaction experiment is described in the following. In the steady state experiments, the evaporator and reactor pipes were first heated by the electric heater bands so that the temperatures measured at the locations of 4.6D upstream of the baffle rear surface and $x/D$=4.11 reached 200°C and 600°C, respectively. Then, the heaters attached to the reactor were turned off and the fuel and air were supplied to the reformer. Note that the heaters of the evaporator were powered during the experiment and the temperature inside the pipe was kept at 200°C.

In the unsteady experiment, same as the steady state experiment, the fuel and air were supplied after the evaporator and reactor were heated up to 200°C and 600°C, respectively. The reactor was operated under the initial condition until the temperature characteristics were confirmed to be in steady state (approximately 3000s later). The flow rates of the fuel and air were, then, changed to the secondary condition.

## EXPERIMENTAL CONDITIONS

As described above, experiment was carried out with singe-stage and double-stage reformers under both steady and unsteady state conditions, in the meanings of evaluating the fundamental characteristics of the multi-stage reactor and its performance under load changing conditions.

Table 1 shows the conditions of the experiment of the single-stage reformer. In this case, the fuel and air were both supplied to the reactor from the evaporator through the baffle plate. Namely, no air was injected from the sidewall of the reactor in this case. $Q_{air}$ and $Q_{fuel}$ are the volume flow rates of the air and fuel fed to the evaporator, respectively. Note that $Q_{fuel}$ represents the flow rate of the fuel in liquid form. $\phi_1$ is the equivalence ratio on the bases of the oxidative reaction. The stoichiometric ratio of the POR, therefore, takes place at $\phi_1$=3. $q_e$ is the output power of the electric heater attached to the evaporator. As shown in Table 1, the fuel flow rate, $Q_{fuel}$, was changed under four conditions, and with each $Q_{fuel}$, the air flow rate, $Q_{air}$, was varied in the range of equivalence ratios, $3.0 \le \phi_1 \le 7.0$.

In Table 2 is shown the conditions of the experiment carried out for a double-stage reformer. In this case, additional air was injected to the reactor at the location between the two tube bundles, $x/D$=4.11. The experiment was conducted under three conditions of $Q_{fuel}$. In regard to each $Q_{fuel}$, air was supplied to the evaporator and reactor at the mass flow rate of $Q_{air1}$ and $Q_{air2}$, respectively. The total amount of air provided to the reactor, $Q_{total}=Q_{air1}+Q_{air2}$, was kept constant in each $Q_{fuel}$ case, and the ratio of $Q_{air1}$ and $Q_{air2}$ ($\gamma = Q_{air2}/Q_{air1}$) was changed. Therefore, the equivalence ratio at the first stage, to which fuel and air were supplied from the baffle plate, was varied in the range of $4.5 \le \phi_1 \le 7.0$. Note that

Table 1. Flow rate conditions in singe-stage case.

| case | $Q_{fuel}$ [cm$^3$/s] | $\phi_1$ | $q_e$ [W] |
|---|---|---|---|
| *ss_f1* | 0.066 | 3.0, 3.5, 4.0, 4.5, 5.0, 5.5, 6.0, 6.5, 7.0 | 112 |
| *ss_f2* | 0.092 | | 151 |
| *ss_f3* | 0.122 | | 201 |
| *ss_f4* | 0.145 | | 270 |

Table 2. Flow rate conditions in double-stage case.

| case | $Q_{fuel}$ [cm$^3$/s] | $\phi_{total}$ | $\phi_1$ |
|---|---|---|---|
| *ds_f1* | 0.066 | 4.0 | 4.0, 4.5, 5.0, 5.5, 6.0, 6.5, 7.0 |
| *ds_f2* | 0.092 | | |
| *ds_f3* | 0.145 | | |

| $\gamma = Q_{air2}/Q_{air1}$ | $q_e$ [W] |
|---|---|
| 0.0, 0.125,0.25,0.375, 0.50, 0.625, 0.75 | 112 |
| | 151 |
| | 270 |

Table 3. Flow rate conditions in unsteady operation case.

| case | $Q_{fuel}$ [cm$^3$/s] | $\phi_1$ | identical case | |
|---|---|---|---|---|
| *uo_ss* | 0.066 | 4.0 | = ss_f1 | → |
| *uo_ds* | 0.066 | | = ss_f1 | |

| | $Q_{fuel}$ [cm$^3$/s] | $\phi_{total}$ | $\phi_1$ | identical case |
|---|---|---|---|---|
| → | 0.145 | 4.0 | 4.0 | = ss_f4 |
| | 0.145 | 4.0 | 5.0 | = ds_f3 |

the total equivalence ratio of the whole reformer, $\phi_{total}$, calculated from the values of $Q_{total}$ and $Q_{fuel}$ , was kept at 4.0.

Table 3 tabulates the conditions of the unsteady experiment. The experiment was conducted by first running the reformer in a steady operation under the initial condition, and then changing the condition to the secondary one. Two cases were tested. One is by starting the reformer under an initial condition of $Q_{fuel}$=0.066cm$^3$/s and $\phi_1$ =4.0 both supplied in a single-stage form, which was identical to that in case ss_f1. Then $Q_{fuel}$ and $Q_{air}$ were changed to $Q_{fuel}$=0.145 cm$^3$/s and $Q_{air}$=151 cm$^3$/s both supplied again in a singe-stage fashion. This condition implies a load change from single- to single-stage case keeping $\phi_1$ constant at $\phi_1$=4.0. The other is by starting the experiment under the same initial condition mentioned above, and then supplying the fuel and air in a double-stage fashion. In this case, $Q_{fuel}$, $Q_{air1}$ and $Q_{air2}$, were 0.145, 100 and 51cm$^3$/s, respectively, i.e., the equivalence ratios were $\phi_1$=5.0 and $\phi_{total}$=4.0. In this experiment, measurements of the instantaneous temperature distributions and gas sampling at the time period of 0, 10, 30, 60, 90, 120, 180, 600 and 2000s after changing the condition were carried out.

## RESULTS AND DISCUSSION

Here are discussed the results of the multi-stage reformer under the conditions of single-stage, double-stage and unsteady state conditions. Before moving on to the discussion, several parameters that are used in discussing the characteristics of the reformer are introduced here.

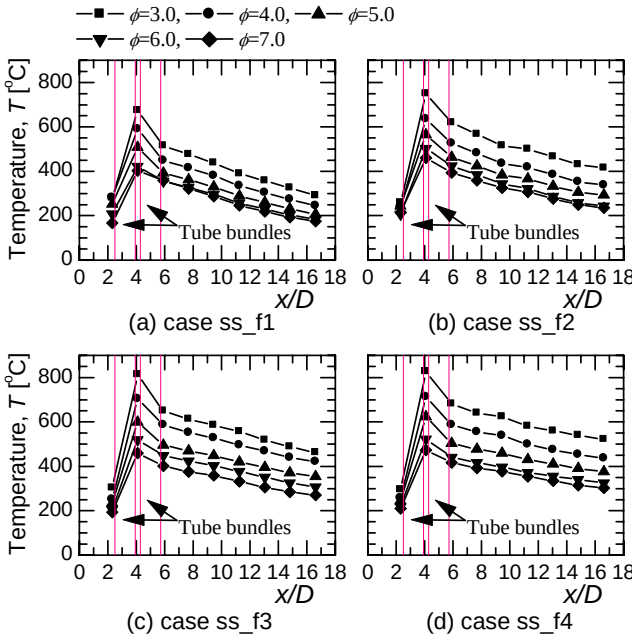


Fig. 5. Streamwise temperature distributions along reactor centerline (case ss_f1~f4).

In the present study, the quantities of the reacted or unreacted methanol cannot be measured directly due to the properties of the column applied to the gas chromatograph and the silica gel chamber, which collects water and methanol. Therefore, these quantities were estimated from the concentrations of other gases included in the exhaust gas.

Since the summation of the concentrations of $H_2$, $N_2$, $O_2$, CO and $CO_2$ in the exhaust gas was 100±2%, the major components of the gas was expected to be these 5 values plus water and methanol that was collected by the silica gel chamber. When paying attention on the carbon atom, the components possessing it among the aforementioned ones are CO, $CO_2$ and methanol. Therefore, the quantity of the reacted methanol can be calculated by Eq. (1) using the concentrations of CO and $CO_2$ in the exhaust gas.

$$\alpha \equiv \frac{M_{CH_3OH,consumed}}{M_{CH_3OH,supplied}} = \frac{M_{CO}+M_{CO_2}}{M_{CH_3OH,supplied}} = \frac{Y_{CO}+Y_{CO_2}}{Y_{N_2}} \times \frac{M_{N_2}}{M_{CH_3OH,supplied}} \quad (1)$$

$M$ is the molar flow rate. $Y_X$ is the concentration of the $X$ component in the exhaust gas. Thus the conversion ratio of methanol, $\alpha$, was defined.

To evaluate the production efficiency of each component, the production rate of component $X$ against 1mol of methanol, $\xi_X$, was defined as Eq. (2).

$$\xi_X \equiv \frac{M_X}{M_{fuel,supplied}} = \frac{(Y_X / Y_{N_2})M_{N_2}}{M_{fuel,supplied}} \quad (2)$$

In calculating the production rate of $H_2O$, $\xi_{H_2O}$, the following assumption was applied: all H atoms belonging to the reacted methanol were used in generating $H_2$ and $H_2O$. $\xi_{H_2O}$ is, thus, obtained by the following equation.

$$\xi_{H_2O} = 2\alpha - \xi_{H_2} \quad (3)$$

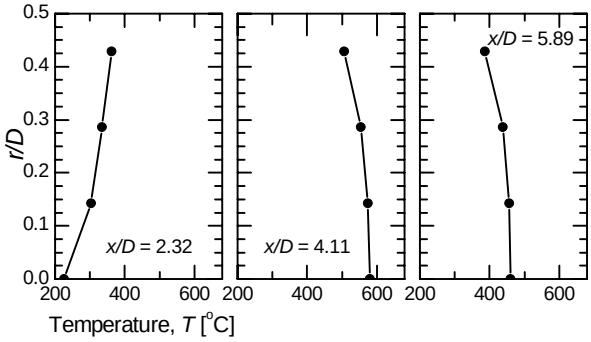


Fig. 6. Radial temperature distributions in the reactor at $x/D$=2.32, 4.11, 5.89 (case ss_f2, $\phi_1$=5.0).

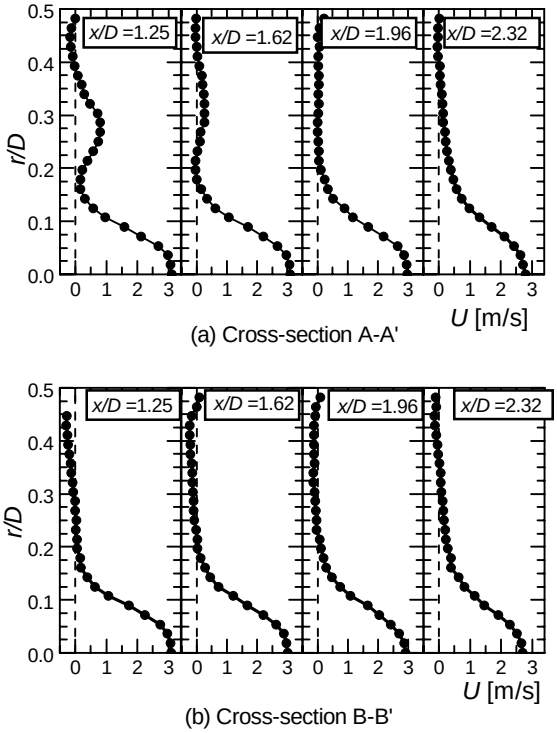


Fig. 7. Cross-sectional distributions of the streamwise velocity in the area downstream the baffle plate (identical flow condition with case ss_f1).

**Single-stage Reformer**

Figure 5 shows the streamwise distributions of the temperature along the reactor centerline in cases ss_f1~4. In Fig. 5(a), the temperature at the location of $x/D$=4.11 takes its maximum value in the case of $\phi_1$=3.0 and decreases as $\phi_1$ increases. This tendency is in common with the temperatures at other locations or in other fuel flow rate cases. This is due to the fact that when $\phi_1$ becomes small, the oxygen supply rate to the methanol increases that results in enhancement of the oxidization reaction and increase of the gas

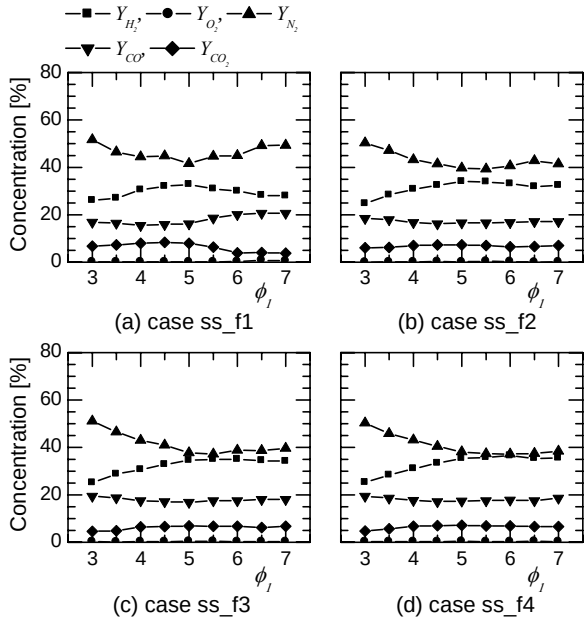


Fig. 8. Relation between concentration and equivalence ratio (cases ss_f1~4).

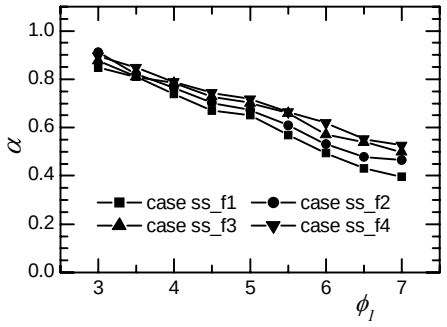


Fig. 9. Conversion ratios of methanol.

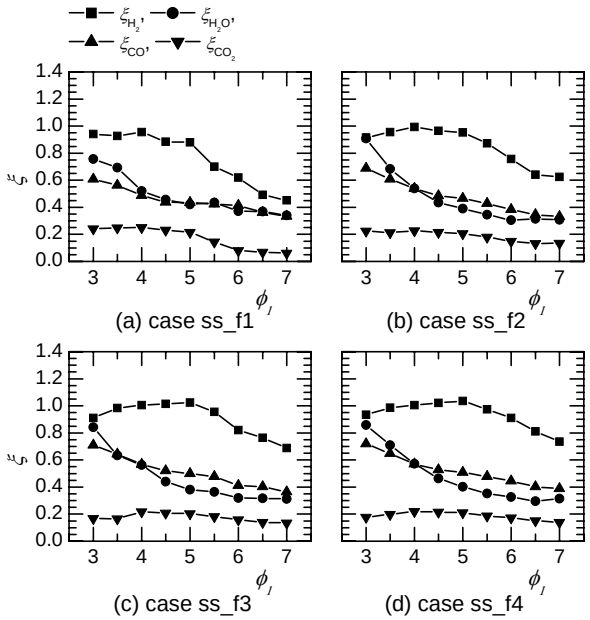


Fig. 10. Mole production rates (cases ss_f1~4).

temperature. In addition to this, since $\phi_1$ was adjusted by changing the air flow rate under a constant fuel flow rate condition, increase of $\phi_1$ leads to a reduction of the total flow rate of the gas supplied to the reactor. In this case, the heat loss from the reactor wall increases. This might be another reason why the temperature decreases under larger $\phi_1$ condition.

The streamwise distributions of the temperature show a common characteristic in all cases, namely, a maximum peak is obtained at the location of *x/D*=4.11 and decreases in the downstream area. It is, therefore, expected that the reaction takes place mainly at the location where the first tube bundle is inserted.

Cross-sectional temperature distributions were measured by traversing the thermocouple probe in the radial direction. Figure 6 shows the results obtained in case ss_f2 of $\phi_1$=5.0. The measured streamwise locations were *x/D*=2.32, 4.11 and 5.89 that correspond approximately to the inlet of the first tube bundle, middle of the first and second bundle and the outlet of the second bundle, respectively.

Figure 7 shows the spanwise distributions of the streamwise velocity at the locations of *x/D*=1.25, 1.62, 1.96 and 2.32, i.e., the area between the baffle plate and first tube bundle, obtained in the LDV measurements. Figures 7(a) and (b) show the results of the cross-sections respectively intersecting the center and midpoint of the surrounding nozzles of the baffle plate (see Fig. 4).

In Fig. 6, at the location of *x/D*=2.32, the temperature takes a minimum peak at the reactor centerline and higher temperature is obtained near the sidewall. In Fig. 7(a), two peaks of *U* are observed at the locations of *r/D*=0 and 2.85. In Fig. 7(b), a maximum peak is obtained at *r/D*=0. These peak locations correspond to the areas in the downstream of the center and surrounding jets. Since the center nozzle has a larger diameter compared with that of the surrounding ones, a jet of large flow rate is produced from the center nozzle. The lower temperature obtained at the centerline is, therefore, attributed to this center jet blowing the mixed gas produced from the evaporator. On the contrary, the reactor wall temperature is increased by the heat produced from the downstream of the reactor. The air near the wall is, hence, heated and a higher temperature is obtained compared with the fluid located near the centerline.

As shown in Fig. 7(a), the surrounding jets diffuse in the downstream, and the velocity decreases as *x/D* increase. In the same area close to the sidewall, flow with negative velocity is obtained in Fig. 7(b). These results indicate that a flow of three-dimensional structure was generated in the downstream area of the baffle plate, and a circulation might exist near the sidewalls due to the interaction between the center jet and surrounding jets. Consequently, most of the fuel-air mixed gas enters the inlet of the first tube bundle in the area near the reactor centerline.

On the other hand, at the outlet of the tube bundles, i.e., *x/D*=4.11 and 5.89 shown in Fig. 6, the temperature takes a maximum peak at the reformer centerline and decreases as it approaches the reactor wall. The temperature increase obtained between *x/D*=2.32 and

*x/D*=4.11 implies that the reaction mainly starts not in the area between the baffle plate and the first tube bundle but inside the first tube bundle. Furthermore, since the maximum peaks of *U* at *x/D*=2.32 and *T* at *x/D*=4.11 are located at the centerline, the reaction is expected to occur in this area.

Figure 8 shows the relation between the concentrations of components in the exhaust gas and equivalence ratio, $\phi_1$. The concentration of $O_2$ is less than 0.2% in all cases indicating that the supplied $O_2$ were totally consumed in the reaction. The concentration of $H_2$ increases as $\phi_1$ increases in the area of $\phi_1$<5.0. However, at $\phi_1$>5.0, the values are constant or, in some cases, slightly decreases as $\phi_1$ increases.

The aforementioned gas concentrations are the values directly obtained from the gas analysis of the exhaust gas. Therefore, effects of the methanol and water removed from the gas are not sufficiently considered. In the following, the characteristics of parameters $\alpha$ and $\xi_X$ described in Eqs. (1) and (2) are discussed.

Figure 9 shows how $\phi_1$ affects the conversion ratio of methanol, $\alpha$. $\alpha$ decreases linearly as $\phi_1$ increases. When $\phi_1$ is small, larger reaction heat is produced due to the increase of the supplied $O_2$ rate. The temperature inside the reactor, therefore, increases as described in Fig. 5, and the decomposition and fully-oxidation reactions of methanol become more active. On the contrary, under larger $\phi_1$ conditions, the air flow rate is reduced that incurs a fuel-rich condition in the reactions including POR and larger heat loss at the reactor walls.

The production ratio, $\xi$, is shown in Fig. 10. In the region of $\phi_1$<5.0, $\xi_{H_2}$ is constant or slightly increases as $\phi_1$ increases, and decreases in the area of $\phi_1$>5.0. Hence, the maximum production ratio of $H_2$ is obtained approximately under the condition of 4.0<$\phi_1$<5.0. When $\phi_1$ is small, a large conversion ratio, $\alpha$, is obtained as shown in Fig. 9. However, oxidization of $H_2$ to $H_2O$ also becomes active due to the high temperature and the concentration of $H_2$ decreases as shown in Fig. 8. On the contrary, under larger $\phi_1$ condition, the conversion rate of methanol becomes small. Thus, a tradeoff matter exists between $\alpha$ and $H_2$-yield. This is believed the be the reason why the maximum peak of $\xi_{H_2}$ is obtained at 4.0<$\phi_1$<5.0

**Double-stage Reformer**

Figure 11 shows the streamwise distributions of the temperature along the reactor centerline obtained in the cases of a double-stage reformer. The results of case ss_f4 of $\phi_1$=4.0 are included in the figure for comparison.

At *x/D*=3.97, the temperature decreases as $\gamma$ increases, and in the downstream area (*x/D*≥6), the temperature increases under larger $\gamma$ conditions. Since the total amount of air supplied to the reactor was fixed in cases ds_f1~3, an increase of $\gamma$, which is the ratio of the air flow rate injected to the second and first stages, implies the increases of $\phi_1$ and air flow rate supplied to the second stage. In the double-stage reformer, the air and fuel were supplied to the first stage in the same way as in the single-stage case, and a common reaction characteristic is expected to take place. The reaction temperature is, therefore, reduced under larger $\phi_1$ condition due to the fuel rich condition obtained in the first stage of the reactor as mentioned in the previous section.

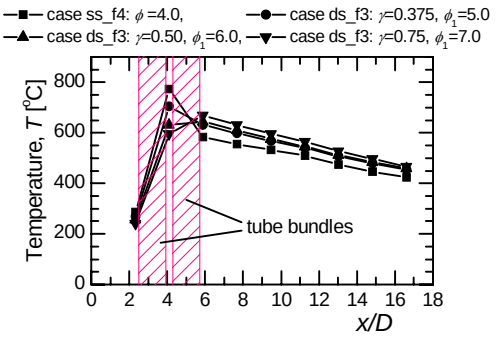


Fig. 11. Streamwise temperature distributions (comparison of cases ss_f4 and ds_f3).

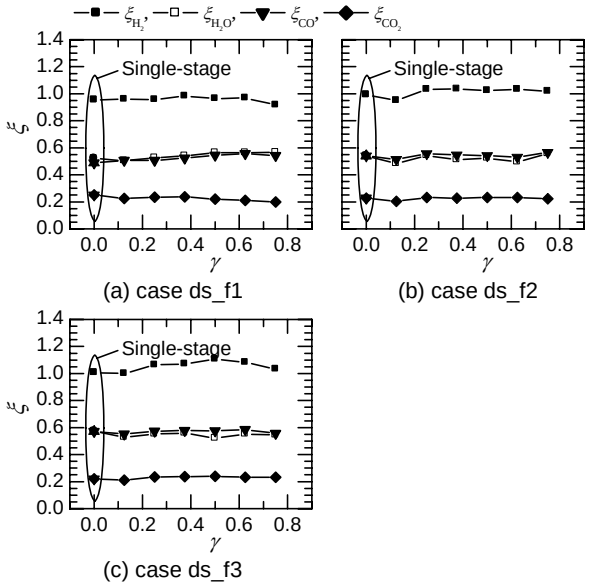


Fig. 12. Relation between $\gamma$ and $\xi$.

On the other hand, as indicated in Fig. 9, larger amount of unreacted methanol enters the second stage in association with the increase of $\phi_1$. In combination with the additional air injected to the second stage, a more active reaction, therefore, takes place in the downstream. This is believed to be the main reason why a higher temperature is obtained in case ds_f3 in the downstream area.

Figure 12 illustrates how $\gamma$ affects $\xi$. The results of the single-stage case are included in the figure for comparison. In cases ds_f1 and ds_f2, the variation of $\xi_{H_2}$ is small against $\gamma$. In case ds_f3, a slight increase of $\xi_{H_2}$ is obtained as $\gamma$ increases in the area of $\gamma$ <0.5, and the difference between the results in cases ss_f4 and ds_f3 is approximately 10%. This implies that the production ratio of $H_2$ is not largely affected by increasing the reformer stage from single- to double-stage: at least the performance of double-stage case is

not inferior to that of the single-stage case in the present study.

Although a noticeable improvement was not achieved in terms of the reaction efficiency by introducing the double-stage reforming, the results obtained in Figs. 11 and 12 indicate the possibility of controlling the temperature of the reformer by multiplying the reaction stages without incurring a serious deterioration of the reforming efficiency. This is important since the reformer can be protected from thermal fatigue by applying an appropriate gas supply ratio and preventing the generation of a significant increase of local temperature.

**Experiment of Load Change in Single-/double-stage Reformers**

In this section, the results obtained in the reformer operating under the condition of load change are discussed. As the load change condition, the fuel flow rate was increased, and the reformer characteristics after the load change were monitored in the experiment. Figures 13 and 14 show the distributions of the temperature and $H_2$ production rate, $\xi_{H_2}$, after the condition was changed. $T_e$ in Fig. 13 is the temperature of the gas in the evaporator. In case uo_ss, the temperature at *x/D*=4.11 increases markedly and reaches 750°C at 250s. On the contrary, in case uo_ds, the temperature difference at the time period of the load change is small. This is considered to be owing to the separation of the air supply into the first and second stages. By dividing the air, the equivalence ratio in the first stage, $\phi_1$, was increased and the reaction temperature was, therefore, decreased. On the other hand, due to the additional air produced to the second stage, the temperature at *x/D*=5.89 was increased, larger in case uo_ds than in case uo_ss.

In Fig. 14, $\xi_{H_2}$ decreases just after the reformer load is changed (*t*=10s). At *t*=30s, $\xi_{H_2}$ continuously decreases in case uo_ss, while in case uo_ds, it makes a relatively quick recovery and increase. As the time proceeds, $\xi_{H_2}$ in case uo_ds shows a larger value and the difference of $\xi_{H_2}$ between the two cases remains almost constant. This result implies the possibility of obtaining a better response by multiplying the reaction process in the reformer.

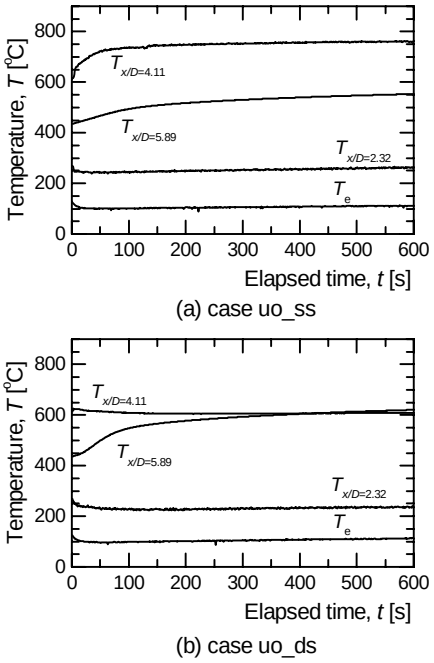


Fig. 13. Temperature profiles after load change (t=0: load change period).

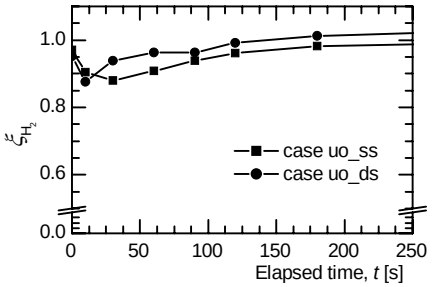


Fig. 14. Time history of $H_2$ production rate after load change.

**CONCLUSIONS**

In the present article, single- and double-stage methanol fuel reformer was experimentally evaluated particularly on the basis of the thermal and reaction characteristics. The major conclusions obtained are listed in the following.

1. A multi-stage reformer consisting of evaporator and reactor was fabricated and operated under the conditions of varying the equivalence ratio, $\phi$, in the range of $3.0 \le \phi \le 7.0$. Hydrogen production and a suitable temperature level for practical use were obtained by the reformer.
2. A better performance was obtained under the conditions of $\phi$=4.5~5.0 than the stoichiometric value of partial oxidation, $\phi$=3, in the present reformer.
3. Most of the reaction was expected to take place inside the first tube bundle due to the effective heat transfer between the fluid and wall that preserves high temperature condition.
4. A maximum peak existed in the $H_2$ production rate per supplied fuel in relation with $\phi$. This is due to the trade-off between the methanol conversion ratio, $\alpha$, and $H_2$-yield.
5. In the double-stage case, temperature control of the reformer was possible without deteriorating the reforming efficiency. Moreover, in some cases, an increase of the $H_2$ production rate by 10% was obtained in this case compared with the singe-stage case.
6. A faster recovery from a temporal decrease of the $H_2$ production performance during the load change of the reformer was obtained in the double-stage case, which indicated that a higher response performance could be achieved in this case than the single-stage case.

**ACKNOWLEDGEMENT**

The work is partially supported by the Mazda foundation, General Sekiyu K.K. research foundation and Japan Society for the Promotion of Science. The authors would like to gratefully acknowledge their support.

**NOMENCLATURE**

$D$ reactor inner diameter, mm
$M$ molar flow rate, mol/s
$q$ heat provided from the heater, W
$Q$ volume flow rate, $cm^3/s$
$r$ radial distance from the reactor centerline, mm
$T$ temperature, °C
$x$ streamwise axis, mm
$Y_X$ volume concentration of component X, %

*Greek symbols*

$\alpha$ methanol conversion rate
$\xi_X$ production rate of component X against supplied fuel flow rate
$\phi_1$ equivalence ratio at the first stage
$\phi_{total}$ equivalence ratio of the whole reformer
$\gamma$ ratio between the air flow rates supplied to the first and second stages

**REFERENCES**

1. A.L. Dicks, Hydrogen Generation from Natural Gas for the Fuel Cell Systems of Tomorrow, J. of Power Sources, 61 (1996), pp. 113-124.
2. L.J. Pettersson and R. Westerholm, State of the Art of Multi-Fuel Reformers for Fuel Cell Vehicles; Problems Identification and Research Needs, Int. J. of Hdyrogen Energy, 26 (2001), pp. 243-264.
3. H. Marsh and D. Thingarajan, AIChE Ammonia Safety Symposium, (1992).
4. M. Dunster and J. Korchnak, Production of Synthesis gas from Hydrocarbonaceous Feedstock, Eur Patent No. 303438, (1989).
5. T. Calcott and T. Deague, US Patent No. 4 042 344 (1977).
6. J. Larminie and A. Dickes, Fuel Cell Systems Explained, John Wiley & Sons Inc. (2003).
7. B. Li, S. Kado and Y. Mukainakano, Temperature Profile of Catalyst Bed during Oxidative Steam Reforming of Methane over Pt-Ni Bimetallic Catalysts, Applied Catalysis A, General 304 (2006), pp. 62-71.
8. C. Pan, R. He and Q. Li, Integration of High Temperature PEM Fuel Cells with a Methanol Reformer, J. of Power Sources, 304 (2006), pp. 392-298.